Barbaros Cetin[1]
Microfluidics & Lab-on-a-chip Research Group,
Mechanical Engineering Department,
İhsan Doğramacı Bilkent University,
Ankara 06800, Turkey
e-mail: barbaros.cetin@bilkent.edu.tr

Mehmet D. Asik
Nanotechnology and Nanomedicine Division,
Hacettepe University,
Ankara 06800, Turkey
e-mail: mehmetdoganasik@gmail.com

Serdar Taze
Microfluidics & Lab-on-a-chip Research Group,
Mechanical Engineering Department,
İhsan Doğramacı Bilkent University,
Ankara 06800, Turkey
e-mail: serdar.taze@bilkent.edu.tr

Design and Fabrication of a Microfluidic Device for Synthesis of Chitosan Nanoparticles

Chitosan nanoparticles have a biodegradable, biocompatible, nontoxic structure, and are commonly used for drug delivery systems. In this study, design, modeling, and fabrication methodology of a microfluidic device for the synthesis of chitosan nanoparticles is presented. In the modeling, 2D flow and concentration field is computed using COMSOL Multiphysics® simulation environment to predict the performance of the device. The microfluidic chip is fabricated out of PDMS. The fabrication of the mold for the microfluidic device is performed using high-precision micromachining. Some preliminary proof-of-concept experiments were performed. It was observed that compared to conventional batch-type methods, the proposed microfluidic device can perform the synthesis much faster and in a much automated and convenient manner. [DOI: 10.1115/1.4026287]

Introduction

Biopolymeric micro and nanoparticles can be vital for various applications in industry, science and medicine. Such as one of the linear biopolymers, chitosan, has become the center of attention for medical and pharmaceutical applications in recent years due to its high biocompatibility and biodegradability [1,2]. Chitosan is a hydrophilic macromolecule which can form biodegradable nanoparticles for site specific delivery of vaccines, genes, drugs and other biomolecules in human body [3]. Moreover, it is used as a topical dressing in wound management due to its hemostatic, stimulation of healing, antimicrobial, nontoxic, biocompatible, and biodegradable aspects [4]. Chitosan has also been considered as a promising candidate for bone tissue engineering since it (i) causes minimal foreign body reactions, (ii) has the ability to be molded into various geometries and forms such as porous structures, and (iii) is suitable for cell ingrowth and osteoconduction [5]. The conventional methods for the formation of chitosan nanoparticles include emulsion droplet coalescence, emulsion solvent diffusion, reverse micellar method, ionic gelation, polyelectrolyte complexation and desolvation [6]. These techniques are batchwise systems, mostly have the principle of dropwise addition of the cross-linker molecules to the chitosan solution or chitosan solution to the cross-linker solution. These conventional techniques usually suffer from aggregation of nanoparticles and labor-intense requires a qualified personnel throughout the process due to the lack of automation. Moreover, reproducibility of the process may also be problematic. One alternative to overcome these issues is to synthesize the chitosan nanoparticles within the microchannels in a continuous flow. In this case, the flow hence the process can be performed in a more controlled manner, the aggregation can be reduced due to the continuous flow nature of the process, and the process can be run autonomously once the required solutions are loaded into the microfluidic channels. Many research groups have worked on microfluidics devices that can produce chitosan micro and nanostructures such as microfibers, microparticles, and nanoparticles [1,7–9]. The integration of microfluidic and particle technologies has given promising results for both inorganic and organic micro and nanoparticles considering the rapid and tunable mixing, adjustable flow rates, and mixing time result in narrow size distribution or distinct shapes with better control of nanoprecipitation process [10].

The main challenge of synthesis is the mixing of the nanoparticles with tripolyphosphate (TPP) solution. Due to low Reynolds number nature (i.e., laminar flow) of the microchannel flows, mixing of species becomes a challenge due to the absence of turbulence. The proper mixing in a microchannel can be achieved with various channel designs (passive mixers) or introducing additional mixers such as ultrasonic mixer, electrokinetic forcing and alternate injection mixer (active mixers) [11]. Although the use of mixer has a positive effect on mixing efficiency, mixers also bring some difficulties such as additional cost and effort to tune the mixer on a microfluidic device. The easy and simple way of an efficient mixing is to utilize special design of the microfluidic network. Different designs have been proposed in the literature such as hydrodynamic focusing channels [11], zigzag microchannel [12], squarewave, three-dimensional serpentine, and staggered herringbone mixer [13].

When the fabrication of the microfluidic devices is concerned, there are basically two common approaches which are direct substrate manufacturing (photolithography, laser ablation, etc.) and mold-based techniques (hot embossing, injection molding, or soft-lithography) [14]. Photolithography has good ability to manufacture very small and complicated microchannel structures, but it usually involves multistep processes which take considerable time, specific chemical requirements especially for etching steps, and more importantly it requires high tech facilities in a cleanroom environment. On the other hand, laser ablation is localized, noncontact removal of the material from the surface by exposing the surface to laser. Unlike photolithography, laser ablation does not require a mask and may be applied to a wide variety of substrate materials [15]. Although the cost of the process is relatively low, the investment cost of the equipment is relatively high. Moreover, generally the surface roughness of the laser ablated channels is not superior than that of mold-based techniques [16]. Mold-based techniques require a mold (sometimes mold is also referred as the mask) to process. Although the fabrication of the mold may need lithography-based, relatively complicated fabrication process; once the mold is fabricated, the mold may well be used for several times. After the completion of the mold, the fabrication procedure is simple and highly reproducible (i.e., low-cost replication), which makes mold-based techniques very suitable for mass production. A common material used in the fabrication of the microchannels is the polydimethylsiloxane (PDMS) due to its

[1]Corresponding author.

Manuscript received November 25, 2013; final manuscript received December 6, 2013; published online January 29, 2014. Assoc. Editor: Sushanta K Mitra.

low cost, low toxity, and transparency. Bonding PDMS with glass is also a straightforward surface treatment process with oxygen plasma.

One alternative to fabricate the microfluidic device is to use mechanical micromachining (i.e., CNC-machining) either for direct substrate manufacturing or for the fabrication of the mold. For the direct substrate manufacturing, the limits of the process are constrained by the size of the milling tool which may lead to unsatisfactory end-product for microfluidic applications. However, for the fabrication of the mold, the limits of the process is constrained with the *xyz*-accuracy of the tool-positioner of a CNC-machine, since the negative of the microfluidic structure is fabricated as a mold. With today's technology, by using magnetic bearings for their positioning systems, the *xyz*-accuracy of a conventional CNC-machines are around 5 μm. Therefore, a mold can be fabricated using mechanical machining in the order of hours without any need for clean-room equipment within the desirable accuracy limits for microfluidic devices. Moreover, CNC-machining can generate 3D structures without any difficulty (this is also doable with lithography-based methods with some additional steps, not straightforward though [15]). Common mold materials for mold-based techniques are silicon (quartz/glass), SU-8 photo-resist, polymer based materials (e.g., plexiglas) or any metal-based materials (titanium, stainless steel, etc.). Polymer- and metal-based mold materials are superior over silicon or photo-resist based mold materials in terms of the durability and robustness. In the case of mechanical micromachining, any of these materials can be selected. However, machinability, cost, and the expected life-span of the mold are the important parameters which need to be considered during the selection of the mold material. Another important parameter is the expected life of the mold. Considering the use of the mold to produce more than 7000–10,000 parts, metal-based materials are the best choice. However, using metal-based materials comes with a price. Metal-based materials' machining is costly due to the reduced tool life and the increased machining time. On the other hand, machining of polymer based materials (PMMA, plexiglass, etc.) is less problematic in terms of tool life and machining time, yet the mold still can be used for many times.

The major objective of this study is to utilize microfluidic network for the synthesis of chitosan nanoparticles. The design and fabrication methodology of the microfluidic chip, and the preliminary experimental results are presented. A microfluidic device for synthesis of chitosan nanoparticles was proposed in the literature [10] without any mixing mechanism. In this study, micro obstacle structures as proposed in Ref. [17] are introduced within the microfluidic network to enhance the mixing of the solutions, hence the device performance. The synthesis of chitosan nanoparticles is performed in two units in parallel with four inlet ports and two exit ports. S-shaped channels are used to increase the length of the mixing section, hence the efficiency of the mixing without using excessive chip area. To predict the performance of the device, a numerical model which models the fluid flow and the mixing of the two solutions within the microchannel is developed. In order to be able to fabricate relative high aspect ratio obstacles within the microchannels, high-precision micromachining is utilized for the fabrication of the mold of the microfluidic device. With the current dimensions, the proposed device enables a relatively high throughput compared to the typical microfluidic devices.

Modeling and Design

The assessment of the mixing efficiency for different channel structures were discussed previously by the same group [18], and the existence of the micro obstacle structures within the channel were shown to enhance the mixing efficiency. As a consequence of that study, a microfluidic channel network with five inlet reservoirs (one for TPP solution, reservoir **A**, four for chitosan solution, reservoirs **B**) and two exit reservoirs (reservoirs **C**) is

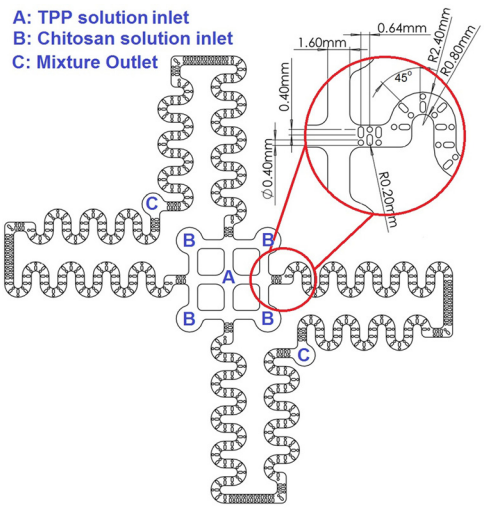

Fig. 1 Drawing of the microfluidic device

proposed for the synthesis of chitosan nanoparticles as shown in Fig. 1 which runs the mixtures in four microchannels in parallel. The width of the channels are 1600 μm and the micro obstacles composed of circular and elliptic geometries with a diameter of 400 μm. The total length of the one S-shaped channel (from inlet to exit) is about 7 cm.

Following the well-known ionic gelation method, the synthesis requires mixing of acetic acid based chitosan polymer solution with the water based TPP solution with a certain ratio. In a typical ionic gelation chitosan nanoparticle synthesis, mixing ratio of TPP:chitosan ratio varies in between 1:2 to 1:5. In this study, the mixing ratio of 1:4 is used. For an efficient synthesis, the mixing needs to be complete. To quantify the mixing, the concentration field together with the flow fields needs to be computed. In the computation, following assumptions are used:

(1) the working fluids are incompressible, Newtonian liquids,
(2) the gravitational effects and buoyancy effects are negligible,
(3) both species have identical diffusion coefficients,
(4) no chemical interaction between the chitosan particles and the channel walls,
(5) no chemical reactions take place,
(6) the mixing of two liquids ensures the mixing of chitosan nanoparticles with TPP, and
(7) the formation of the nanoparticles does not change the viscosity of the solution.

The flow field is governed by Navier–Stokes equation

$$\rho_m \mathbf{u} \cdot \nabla \mathbf{u} = -\nabla P + \mu \nabla^2 \mathbf{u} \tag{1}$$

subjected to the no-slip boundary conditions at the channel walls, specified flow rates at the reservoirs, and zero pressure boundary condition at the exit. The concentration field is governed by convection-diffusion equation

$$\mathbf{u} \cdot \nabla c = D \nabla^2 c \tag{2}$$

subjected to insulated boundary at the channel walls and the specified concentration at the reservoirs. In here, c represents the dimensionless mole fraction of the acetic acid. Therefore, c is assigned as unity at the inlets of acetic acid, and assigned as zero for the inlets of the water. At the exit, convective flux boundary condition is assigned.

In these equations, mixture density and mixture viscosity need to be described in terms of the concentration. The mixture density can be determined by using the following relation [19]:

$$\rho = A_o + A_1 T + A_2 T^2 + A_3 T^3$$
$$A_o = 534.613 + 1950.54c - 1054.32c^2 + 174.019c^3$$
$$A_1 = 4.1946 - 10.5253c + 3.15922c^2 \quad (3)$$
$$A_2 = -0.0113495 + 0.0212374c - 0.0036607c^2$$
$$A_3 = 8.43584 \times 10^{-6} - 1.47636 \times 10^{-5} c$$

To determine the mixture viscosity, following relation which relates the water–acetic acid mixture as a function of mole fraction of acetic acid is used [20]:

$$\ln \mu = B_o + B_1/T + B_2 \ln T + B_3 P$$
$$B_o = -9.84679 + 5.93224c - 0.0724913c^2 + 1.59018c^3$$
$$B_1 = 2361.48 + 202.364c - 1594.8c^2 \quad (4)$$
$$B_2 = 0.00609668 - 0.00856923c$$
$$B_3 = 0.014739$$

The lowest temperature was given in Ref. [20] was 313 K, so the same temperature is used in this study. The pressure value is taken as 100 kPa, since the typical pressure drops in liquid microfluidic applications are in the order of 100 Pa [17], the variation of viscosity with pressure is neglected.

In order to quantify the mixing performance, the mixing efficiency at the exit of the mixing section is determined. Mixing efficiency can be determined as [21]

$$\eta_m = 1 - \frac{\int_A |c - c_\infty| dA}{\int_A |c_o - c_\infty| dA} \quad (5)$$

where c is the sample concentration, and c_o and $c_\infty (= 0.8)$ are the sample concentrations in the completely unmixed and completely mixed conditions, respectively. Therefore, $\eta_m = 0$ indicates a completely unmixed state, and $\eta_m = 1.0$ indicates complete mixing.

The density of the water and the acetic acid were taken as 1000 kg/m^3 and 1050 kg/m^3, respectively. Binary diffusion coefficient is taken as 1×10^{-9} m^2/s which a typical value for aqueous solutions [17]. Commercial analysis software, COMSOL Multiphysics®, which is based on the finite element method, was used to determine the flow and concentration fields. Since the density and the viscosity of the fluid depend on the concentration of the acetic acid, and the velocities in x- and y-directions are required to determine the convective terms in the convection-diffusion equation, the flow field and concentration field are coupled. Moreover, the problem becomes nonlinear. Since the equations are coupled and nonlinear, it was observed that the convergence of the solution is sensitive to initial guess. Therefore, to obtain the converged solution, the equations were solved in sequence by updating the initial guess from the previous run. First, the convection-diffusion module was solved based on the initial zero velocities (i.e., purely diffusion equation). After that the incompressible Navier–Stokes module together with the results that were obtained from the diffusion equation is computed. For these initial computations, linear solver is used for both modules. Then, the convection-diffusion and incompressible Navier–Stokes equations were solved in an iterative manner with the nonlinear solver, until the solutions converged. The convergence criteria for the computations were the relative error for the concentration field is below 1×10^{-3}. The simulations were performed on an HP Z400 Workstation (Intel Xeon W3550, Quad core, 3.06 GHz, 16GB RAM).

Three cases were simulated. The ratio was set to 1:4, and the volumetric flow rate of the TPP solution was chosen as 64 ml/min (case #1), 16 ml/min (case #2), and 4 ml/min (case #3), in these three cases. Since the length of the channels are long compared to the width of the microchannel, with the current workstation, the 3D simulation was found to be infeasible. Therefore, only 2D simulations were performed to obtain qualitative results. During the simulations, it was observed that, the convergence and the accuracy of the solution strongly depends on the mesh resolution. If an appropriate mesh resolution is not chosen, the concentration field is found to be completely mixed after the first couple hurdles which is not physical. Therefore, during the mesh generation step maximum mesh size of 20 μm and the minimum mesh size of 10 μm was set both for the domain and the boundaries. With this mesh resolution, number of degrees of freedom was approximately 1 M for concentration and 3 M for the velocity fields. The computational time for each case depended on the number of iterations, and it was observed that number of iterations were higher for the case with higher volumetric flow rate, since the Reynolds and Peclet numbers of the flow, hence the nonlinearity increases. For the case with largest flow rate, the typical computation time was around 25 min. For the 2D simulations, average velocity corresponding to the 3D case was assigned as the average velocity at the inlets, and fully developed conditions were assigned by defining laminar inflow boundary condition.

The concentration field for three cases can be seen in Fig. 2. As seen from the figure, since the flow is laminar, as the volumetric flow rate decreases, there is more time for the solutions to diffuse into each other. Therefore, case #3 has a better mixing performance. To demonstrate this effect, the concentration profile at the exit of the channel is also illustrated in Fig. 3. From this figure, it is clear that among three cases, case #3 has the concentration profile at the exit which is closest to the complete mixed case. To quantify this result, the mixing efficiency of three cases is also calculated. To determine the case for completely unmixed state (c_o), the simulation is performed with very small diffusion coefficient. It was found that mixing efficiency was 71% for case #1, 71% for case #2, and 79% for case #3.

Fabrication of the Device

For the fabrications of the microchannel network, the micromachining facility of Bilkent University Micro System Design and Manufacturing Center was used. A plexiglass mold was

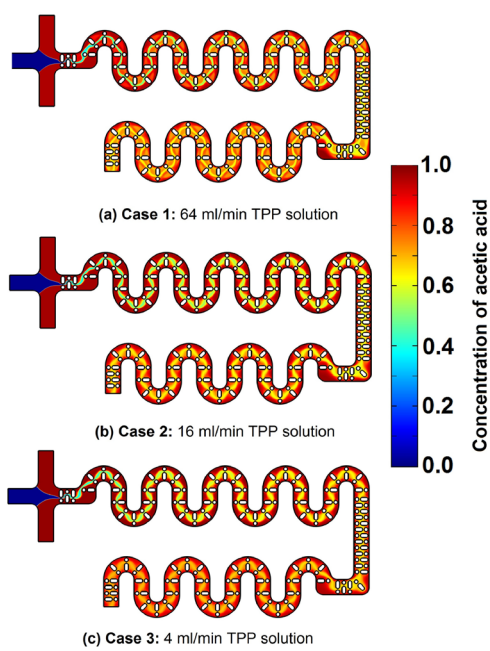

Fig. 2 Concentration field

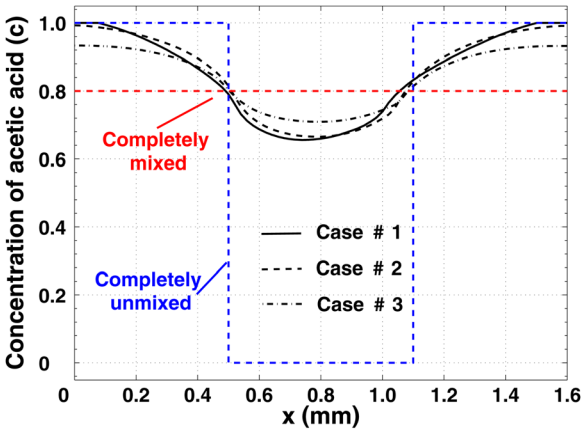

Fig. 3 Concentration profile at the exit

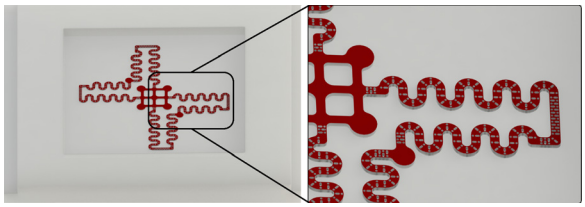

Fig. 4 CAD drawing of the mold

Table 1 Machining parameters

Spindle speed	Maximum 1500 rpm
Tools	Diameter 1 mm and 2 mm and 5 mm end mill Diameter 0.4 mm drill Diameter 20 mm and 80 mm end mill
Material of the tool	Tungsten carbide, high speed steel
Number of teeth	2
Axial depth of cut	50 μm

micromachined and the microchannel network was fabricated out of PDMS and sealed with glass substrate. The fabrication of the device starts with creation of the CAD model of the system. CAD model of the mold can be seen in Fig. 4. The overall dimensions of the model are 120 mm (L) × 120 mm (W) × 20 mm (H). The height of the cavity is 5 mm. CNC-based micromachining was used to fabricate the mold structure out of plexiglas. For the ease of removal of the PDMS from the mold, fillet corners with a diameter of 2 mm were used. Micromachining was performed by a three-axis CNC milling machine (DECKEL MAHO HSC55, Germany). The machining parameters used for the machine are tabulated in Table 1. The steps of the machining process of the mold can be summarized as follows:

(1) Face milling operation, in order to be sure that stock face is smooth and flat (80-mm-diameter tool, spindle speed: 3000 rpm, feed rate: 800 mm/min).
(2) Outside of the stock was machined to final dimensions by contour milling operation (20-mm-diameter tool, spindle speed: 6000 rpm, feed rate: 1250 mm/min).
(3) For handling the mold part, two sides of the stock were machined to final dimensions by counter milling operation (20-mm-diameter tool, spindle speed: 6000 rpm, feed rate: 1250 mm/min).
(4) Milling of the primary molding cavity up to 4.5 mm depth (5-mm-diameter tool, spindle speed: 8000 rpm, feed rate: 1000 mm/min).

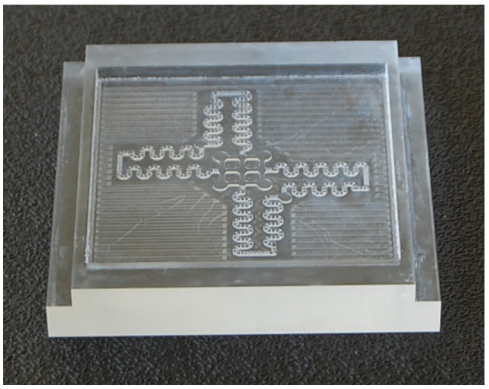

Fig. 5 Photograph of the mold

Table 2 Measured mold dimensions

Depth of holes	500 μm ± 50 μm
Hole diameter	400 μm ± 10 μm
Slot diameter	400 μm ± 10 μm
Slot length	800 μm ± 10 μm
Channel width	1600 μm ± 20 μm

(5) Drilling of the 0.4 mm diameter holes and slots (400-μm-diameter tool, spindle speed: 15,000 rpm, feed rate: 20 mm/min).
(6) Pocket milling, to open mold cavity:
Rough machining at the outside of the channel (2-mm-diameter tool, 12,000 rpm, feed rate: 350 mm/min).
Finishing operation at the near and inside of the channel (1-mm-diameter tool, spindle speed: 12,000 rpm, feed rate: 50 mm/min).

Total machining time took approximately 240 min. Figure 5 shows the manufactured plexiglas mold. To check the accuracy of the machining, the dimensions of the structures within the mold were measured using optical measurement microscope (Vision Engineering Hawk 200) and tabulated in Table 2.

After the fabrication of the mold, PDMS and curing agent were mixed in the ratio of 10:1, and poured into the mold. The microfluidic chip was placed in an oven to cure the PDMS (75 °C for 90 min). After curing, PDMS was peeled off from the mold. The reservoirs were punched out. A clean glass slide and the PDMS were plasma treated, and bonded to get the final device. The final device was checked under the microscope to see any fabrication defects. Finally, water was loaded to the system to check the bonding and any possible leakage. The water and ink mixture was also tested. The system was free of defects, and no leakage was observed.

Experimentation

The microfluidic device is shown on Fig. 6(*a*). The chitosan solution (%0.5 low molecular weight chitosan in %1 acetic acid solution) and water based TriPolyPhosphate solution prepared following the typical procedure and loaded in regular 1-ml syringes (1 syringe for TPP solution, 4 syringe for chitosan solution), placed at the inlet of the channels. Two 2.5-ml syringes are placed at the exit reservoirs to generate negative pressure at the outlets. First, the air is sucked out from the microchannel by the syringes at the exit reservoirs, and then the solutions are introduced within the channel slowly by the syringes at the inlet reservoirs. The pumping of the mixtures was made by pushing the syringes at the inlet and the pumping took 15 s. Once the mixtures flew in the channel, the products were collected from the exit reservoirs, and put in a 2-ml tube and washed. In the washing step,

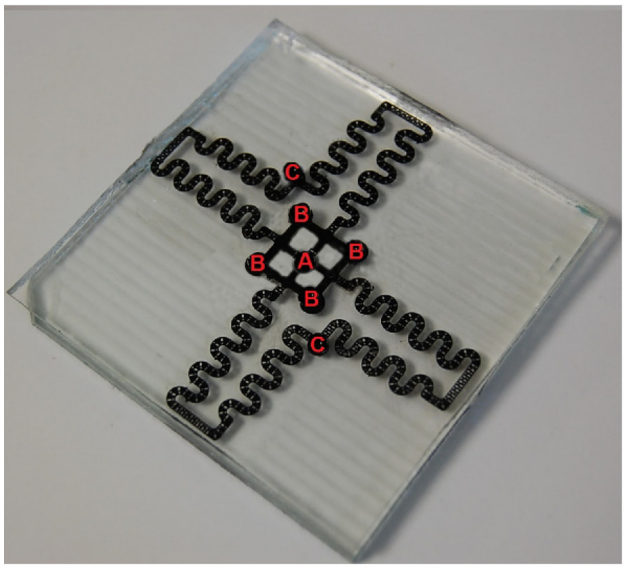

(a)

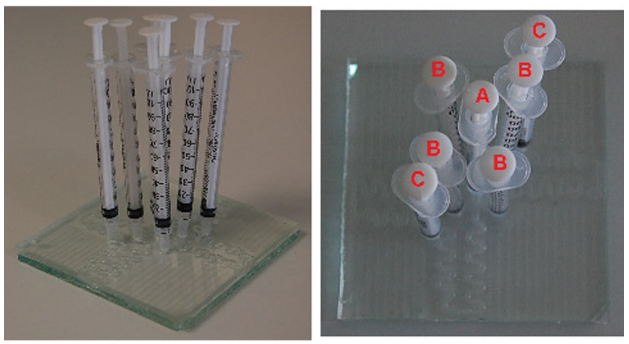

(b)

Fig. 6 (*a*) Photograph of the microfluidic device and (*b*) photograph of the experimental setup

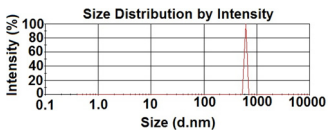

Fig. 7 Result from the zeta sizer

the sample is centrifuged (12,000 rpm for 15 min), supernatant is removed, and 2 ml distilled water is added. This procedure was repeated three times. Then, 1 ml sample was taken to be analyzed with zeta sizer (3000 HSA, Malvern, England, using DLS method). Sample was analyzed for the size distribution. The result of the zeta sizer can be seen in Fig. 7. As seen from the figure, nanoparticles with a size of 550–700 nm were successfully synthesized.

As the last step, a 10 μl droplet was dried out to be analyzed under AFM (NMI AFM, Nanomagnetics, Turkey). An area of 10 μm $\times$ 10 μm is scanned under AFM with a scanning velocity of 1 μm/s. The AFM image of the sample can be seen in Fig. 8. Our primary results showed that we dramatically reduced the production time and produced nanoparticles with a narrow size distribution compared to the conventional methods, on the other hand, contrarily to zeta-sizer results, AFM results showed that aggregations occur during or after the production. A possible cause for the aggregation may be the drying process before the AFM scans. These results suggest that mixing needs be increased to avoid

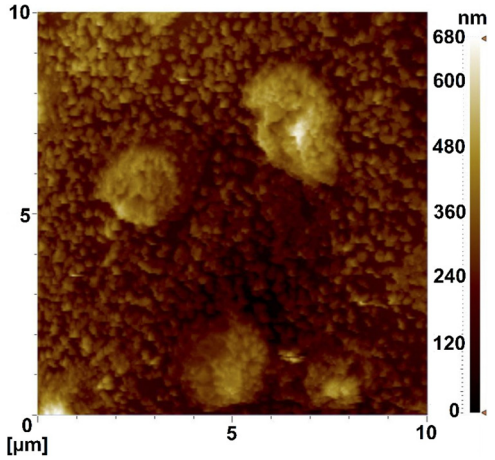

Fig. 8 AFM image of the nanoparticles

aggregation and nanoparticles need to be separated with an alternative technique rather than centrifuging.

Summary and Future Works

In this study, a microfluidic device for the synthesis of chitosan nanoparticles is proposed. The design and fabrication methodology of the microfluidic chip, and the preliminary experimental results are presented. To predict the performance of the device, a 2D numerical model is developed. The fabrication of the mold for the microfluidic device is performed using high-precision micromachining. It was observed that relatively high aspect ratio micro obstacles were able to be fabricated without any major problems with micromachining which would be problem with lithography-based microfabrication techniques. Proof-of-concept experiments were performed to show the synthesis of the chitosan nanoparticles. It was observed that compared to conventional batch-type methods, the microfluidic device can perform the synthesis much faster and in an automated and more convenient manner. The current device has relatively large dimensions compared to the conventional microfluidic devices. With the utilization of the mechanical micromachining the size of the microchannels can be further scaled up to come up with a high throughput device which can be used to synthesize bulk amount of chitosan nanoparticles for clinical/industrial applications. However, a systematic set of experiments needs to be performed to explore the relation between the mixing efficiency, volumetric flow rate, and the size, and the quality of the nanoparticles which will be our future research direction.

Acknowledgment

The authors gratefully acknowledge the financial support for the fabrication of the mold and the financial support for Mr. Serdar Taze by Bilkent University Mechanical Engineering Department.

Nomenclature

A_o = coefficient used in Eq. (3)
A_1 = coefficient used in Eq. (3)
A_2 = coefficient used in Eq. (3)
A_3 = coefficient used in Eq. (3)
B_o = coefficient used in Eq. (4)
B_1 = coefficient used in Eq. (4)
B_2 = coefficient used in Eq. (4)
B_3 = coefficient used in Eq. (4)
c = sample dimensionless concentration
c_o = completely unmixed sample concentration
c_∞ = completely mixed sample concentration

D = diffusion coefficient
P = pressure
T = temperature
$\mathbf{u}$ = velocity vector
η_m = mixing efficiency
μ = viscosity of the mixture (mPa s)
ρ = mixture density

References

[1] Lee, K. H., Shin, S. J., Kim, C.-B., Kim, J. K., Cho, Y. W., Chung, B. G., and Lee, S.-H., 2010, "Microfluidic Synthesis of Pure Chitosan Microfibers for Bio-Artificial Liver Chip," Lab Chip, **10**, pp. 1328–1334.

[2] Muzzarelli, R. A. A., 2011, "Biomedical Exploitation of Chitin and Chitosan Via Mechano-Chemical Disassembly, Electrospinning, Dissolution in Imidazolium Ionic Liquids, and Supercritical Drying," Mar. Drugs, **9**, pp. 1510–1533.

[3] Mahapatro, A., and Singh, D. K., 2011, "Biodegradable Nanoparticles are Excellent Vehicle for Site Directed In-Vivo Delivery of Drugs and Vaccines," J. Nanobiotechnol., **9**(55), pp. 1–11.

[4] Dai, T., Tanaka, M., Huang, Y.-Y., and Hamblin, M. R., 2011, "Chitosan Preparations for Wounds and Burns: Antimicrobial and Wound-Healing Effects," Expert Rev. Anti–Infect. Ther., **9**(7), pp. 857–879.

[5] Venkatesan, J., and Kim, S.-K., 2010, "Chitosan Composites for Bone Tissue Engineering—An Overview," Mar. Drugs, **8**, pp. 2252–2266.

[6] Grenha, A., 2012, "Chitosan Nanoparticles: A Survey of Preparation Methods," J. Drug Targeting, **20**(4), pp. 291–300.

[7] Majedi, F. S., Hasani-Sadrabadi, M. M., Emami, S. H., Taghipoor, M., Dashtimoghadam, E., Bertsch, A., Moaddel, H., and Renaud, P., 2012, "Microfluidic Synthesis of Chitosan-Based Nanoparticles for Fuel Cell Applications," Chem. Commun., **48**, pp. 7744–7746.

[8] Majedi, F. S., Hasani-Sadrabadi, M. M., Hojjati Emami, S., Shokrgozar, M. A., VanDersarl, J. J., Dashtimoghadam, E., Bertsch, A., and Renaud, P., 2013, "Microfluidic Assisted Self-Assembly of Chitosan Based Nanoparticles as Drug Delivery Agents," Lab Chip, **13**, pp. 204–207.

[9] Yang, C.-H., Lin, Y.-S., Huang, K.-S., Huang, Y.-C., Wang, E.-C., Jhong, J.-Y., and Kuo, C.-Y., 2009, "Microfluidic Emulsification and Sorting Assisted Preparation of Monodisperse Chitosan Microparticles," Lab Chip, **9**, pp. 145–150.

[10] Karnik, R., Gu, F., Basto, P., Cannizzaro, C., Dean, L., Kyei-Manu, W., Langer, R., and Farokhzad, O. C., 2008, "Microfluidic Platform for Controlled Synthesis of Polymeric Nanoparticles," Nano Lett., **8**(9), pp. 2906–2912.

[11] Suh, Y. K., and Kang, S., 2010, "A Review on Mixing in Microfluidics," Micromachines, **1**(3), pp. 82–111.

[12] Mengeaud, V., Josserand, J., and Girault, H. H., 2002, "Mixing Processes in a Zigzag Microchannel: Finite Element Simulations and Optical Study," Anal. Chem., **74**(16), pp. 4279–4286.

[13] Liu, Y., Kim, B., and Sung, H., 2004, "Two-Fluid Mixing in a Microchannel," Int. J. Heat Fluid Flow, **25**, pp. 986–995.

[14] Lin, Y.-S., Yang, C.-H., Wang, C.-Y., Chang, F.-R., Huang, K.-S., and Hsieh, W.-C., 2012, "An Aluminum Microfluidic Chip Fabrication Using a Convenient Micromilling Process for Fluorescent Poly(DL-Lactide-Co-Glycolide) Microparticle Generation," Sensors, **12**, pp. 1455–1467.

[15] Nguyen, N.-T., and Wereley, S. T., 2006, *Fundamentals and Applications of Microfluidics*, Artech House, Norwood, MA, pp. 49–50, 67–135.

[16] Becker, H., and Locascio, L. E., 2002, "Polymer Microfluidic Devices," Talanta, **56**, pp. 267–287.

[17] Bhagat, A. A. S., and Papautsky, I., 2008, "Enhancing Particle Dispersion in a Passive Planar Micromixer Using Rectangular Obstacles," J. Micromech. Microeng., **18**, pp. 1–9.

[18] Cetin, B., Taze, S., Asik, M. D., and Tuncel, S. A., 2013, "Microfluidic Device for Synthesis of Chitosan Nanoparticles," ASME 2013 Fluid Engineering Division Summer Meeting, Incline Village, NV, July 7-11, ASME Paper No. FEDSM2013-16349.

[19] Sun, T., Ly, D., and Teja, A. S., 1995, "Densities of Acetic Acid + Water Mixtures at High Temperatures and Concentrations," Ind. Eng. Chem. Res., **34**, pp. 1327–1331.

[20] Qiao, Y., Di, Z. G., Ma, Y. G., Ma, P. S., and Xia, S. Q., 2010, "Viscosities of Pure Water, Acetic Acid + Water, and p-Xylene + Acetic Acid + Water at Different Temperature and Pressure," Chin. J. Chem. Eng., **18**(3), pp. 446–454.

[21] Chen, C.-K., and Cho, C.-C., 2008, "A Combined Active/Passive Scheme for Enhancing the Mixing Efficiency of Microfluidic Devices," Chem. Eng. Sci., **63**, pp. 3081–3087.